Working Fluid Selection and Technoeconomic Optimization of a Turbocompression Cooling System

Derek Young
Interdisciplinary Thermal Science Laboratory,
Colorado State University,
Fort Collins, CO 80524

Spencer C. Gibson
Interdisciplinary Thermal Science Laboratory,
Colorado State University,
Fort Collins, CO 80524

Todd M. Bandhauer[1]
Interdisciplinary Thermal Science Laboratory,
Colorado State University,
Fort Collins, CO 80524
e-mail: tband@colostate.edu

Low grade waste heat recovery presents an opportunity to utilize typically wasted energy to reduce overall energy consumption and improve system efficiencies. In this work, the technoeconomic performance of a turbocompression cooling system (TCCS) driven by low grade waste heat in the engine coolant of a large marine diesel generator set is investigated. Five different working fluids were examined to better understand the effects of fluid characteristics on system performance: R134a, R245fa, R1234ze(E), R152a, and R600a. A coupled thermodynamic, heat exchanger, and economic simulation was developed to calculate the simple payback period of the waste heat recovery system, which was minimized using a search and find optimization routine with heat exchanger effectiveness as the optimization parameter. A sensitivity study was performed to understand which heat exchanger effectiveness had the largest impact on payback period. Of the five working fluids examined, a TCCS with R152a as the working fluid had the lowest payback period of 1.46 years with an initial investment of $181,846. The R152a system was most sensitive to the two-phase region of the power cycle condenser. The R1234ze(E) system provided the largest return on investment over a ten year lifetime of $1,399,666.
[DOI: 10.1115/1.4041197]

Keywords: waste heat recovery, organic Rankine cycle, vapor compression cycle, technoeconomic analysis, working fluid selection

1 Introduction

Energy producing processes typically reject two-thirds of their input energy as low grade waste heat [1]. Using this wasted heat can provide significant improvements to overall system efficiencies, reduce greenhouse gas emissions to mitigate global warming, and reduce facility expenditures. Diesel generator sets (gensets) are used in areas where access to the electric grid is either intermittent or nonexistent. Large diesel gensets can be found in applications ranging from hospitals and commercial buildings to marine cargo ships. On marine cargo ships, power provided by the diesel gensets is used for propulsion, chilling, and auxiliary electrical systems. The analysis presented here will focus on the recovery of waste heat from marine diesel gensets.

Waste heat from diesel gensets is available in the exhaust gas and in the cooling water. The exhaust is typically high or medium grade waste heat with several contaminants, including NO_x and SO_x, which can make waste heat recovery a significant challenge. Further, the pressure drop from adding heat exchangers and exhaust gas cleaners will impose backpressure on the engine, hindering engine performance. The high temperature of this waste heat stream can also exceed the decomposition temperature of traditional refrigerants, which makes it unusable without an intermediate heat exchanger [2,3]. On the other hand, engine coolant is typically low-grade waste heat (~90 °C), which makes converting it into useful work less efficient, but it does not exceed the decomposition temperature of refrigerants. Furthermore, introducing additional pressure drop in the engine coolant loop does not hamper engine performance, and, because it is in the liquid phase, it has improved heat transfer characteristics relative to the low density exhaust gases.

Some of the power produced by the onboard diesel gensets is used to drive an electrical vapor compression system. By implementing a waste heat driven cooling system, the portion of electrical power that drives the vapor compression refrigeration systems will be displaced, thereby reducing fuel consumption. Several of the most common thermally activated cooling systems include absorption, adsorption, ejector, and organic Rankine-vapor compression (ORVC) refrigeration systems.

In the absorption refrigeration system, a volatile component of a binary fluid is vaporized, condensed, and expanded to provide the desired cooling effect. Most commercially available absorption units use either water-LiBr or ammonia–water for the working fluid pair, and coefficients of performance (COPs) using low grade waste heat are nominally 0.6 [4–11]. For water-LiBr systems, if the waste heat stream is lower than 61 °C and the evaporator temperature is lower than 8 °C, the salt can precipitate out of the working fluid mixture which will inhibit the performance of the absorption system [12,13]. There are a number of research studies and case studies describing the performance of the absorption refrigeration system, but there are fewer investigations regarding their economics. There are a number of studies on the exergoeconomic performance of the absorption system, but provide limited insight into physical component cost [14–16].

The adsorption refrigeration system alternately produces heating and cooling in four steps. Unless multiple beds are utilized, the adsorption refrigerator produces cooling for only half of its total operation time, and it typically has a lower COP (~0.35) than absorption cycles [17–21]. In most commercial adsorption systems, the working fluid is water, which is nontoxic,

[1]Present address: Department of Mechanical Engineering, Colorado State University, 1374 Campus Delivery Fort Collins, CO 80523.

Contributed by the Heat Transfer Division of ASME for publication in the Journal of Thermal Science and Engineering Applications. Manuscript received January 6, 2018; final manuscript received July 24, 2018; published online September 12, 2018. Assoc. Editor: Amir Jokar.

noncorrosive, and does not contribute to ozone depletion or global warming. Similar to absorption systems, there are very few studies on economic performance of adsorption refrigeration systems in the open literature [22,23].

Ejector refrigeration systems have a power cycle and a cooling cycle which use the same working fluid. Ejector cycles have a lower COP (0.2–0.4) than the other cycles but have no moving parts, which make the system less complex [24,25]. The nozzle in the ejector cycle cannot operate efficiently over a range of design conditions, which has a detrimental effect on overall cycle performance [26]. A number of exergetic performance studies have been performed on the ejector cycle, but the studies lack detailed component cost modeling. From these studies, it was found that the ejector nozzles have the largest exergy destruction and increasing ejector flow improves system performance [27–30].

The ORVC cycle utilizes heat to vaporize a working fluid, which is expanded in a turbine to produce power. The power output of the turbine is used to drive the compressor on the vapor compression cycle (VCC). On the vapor compression cycle, the working fluid is vaporized in an evaporating heat exchanger to provide the desired cooling effect. The isentropic efficiency of the rotating machinery and the power transfer efficiency between the turbine and the compressor have a significant effect on the overall COP of the ORVC [31]. Again, there is a limited amount of technoeconomic studies performed on combined organic Rankine-vapor compression cycles, but there are several technoeconomic studies on organic Rankine cycles (ORCs) [32,33].

The present study examines a turbocompression cooling system (TCCS) driven by low grade waste heat available in diesel engine coolant onboard large marine cargo ships. Similar to ORVC systems, the TCCS combines an ORC and VCC directly coupled via a high efficiency centrifugal turbocompressor, as shown in Fig. 1. The turbine and the compressor share the same shaft, which is the power transfer mechanism. The turbine and the compressor are hermetically sealed so the system can use different working fluids on the power cycle (ORC) and cooling cycle (VCC) to simultaneously maximize the efficiency of both the turbine and the compressor.

A recent study focused on the technoeconomic performance of the turbocompression cooling system utilizing waste heat in the coolant of large marine diesel generators [34]. The amount of savings provided by reducing fuel consumption was calculated and the simple payback period of the turbocompression cooling system was determined. The current study extends and expands upon this previous analysis to include multiple working fluids to better understand the role of fluid properties on system performance and the payback period.

2 Methods

The turbocompression cooling system in this work was driven by waste heat in hot engine coolant from a large marine diesel generator to provide shipboard cooling, and the inputs for the model are shown in Table 1. In this case, it was assumed that the diesel generators had a total capacity of approximately 35 MW, with 2 MW of waste heat available in the engine coolant at all times. The engine coolant flow rate was 78.5 kg s^{-1} and the inlet

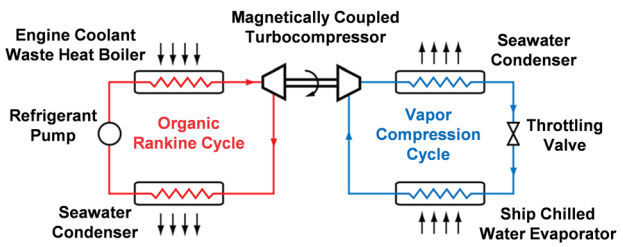

Fig. 1 Process flow diagram for a liquid coupled TCCS

Table 1 Constants inputs to the coupled thermodynamic, heat exchanger, and economic model

Fixed inputs	Value
$T_{boiler,i}$	90 °C
$\dot{m}_{boiler}$	78.5 kg s^{-1}
Q_{boiler}	2 MW
$T_{seawater,i}$	32 °C
$\dot{m}_{condensingwater}$	250 kg s^{-1}
$T_{chillwater,i/o}$	12 °C/7 °C
Plate length	1.32 m
Plate width	1.17 m
Plate thickness	0.7 mm
Plate spacing	4.5 mm
Header diameter	0.350 m
$\eta_{s,turbine}$	0.80
$\eta_{s,compressor}$	0.80
$\eta_{mechanical}$	0.95
$\eta_{s,pump}$	0.80
$\eta_{generator}$	0.975
$COP_{vc,onboard}$	4
$Q_{LHV,MGO}$	42,806 kJ kg^{-1}
$Cost_{MGO}$	$533 mt^{-1}

temperature was 90 °C in the boiler. The organic Rankine cycle and vapor compression cycle rejected heat to the seawater in condensing heat exchangers, and the seawater temperature was assumed to be 32 °C. This temperature is a conservative estimate based on the typical operating location of large cargo ships. The mass flow rate of the seawater was set based on realistic estimates for cooling water pumps in applications of this scale. The physical dimensions of the heat exchanger plates were estimated from manufacturer datasheets, while the empirical correlations for heat transfer coefficients take into account the heat transfer enhancing geometry on the plates. The isentropic efficiency of the

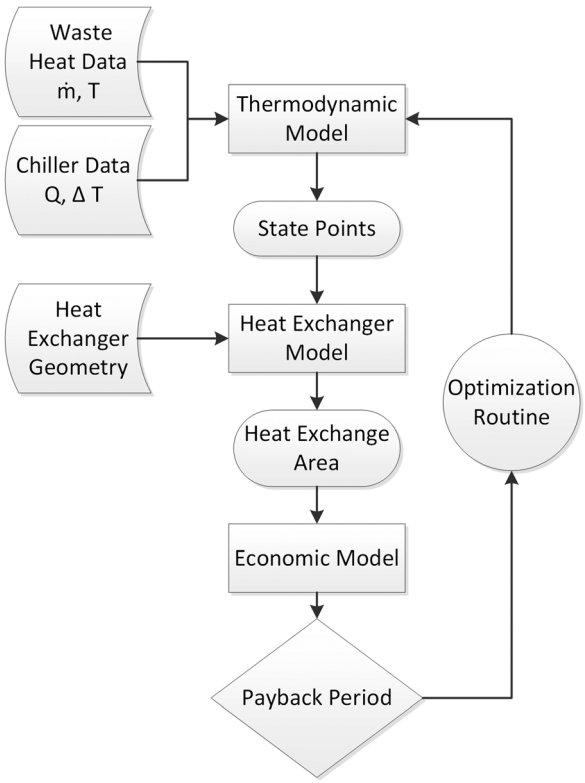

Fig. 2 Block diagram of the modeling approach. The thermodynamic, heat exchanger, and economic model are coupled to perform the optimization and minimize payback period.

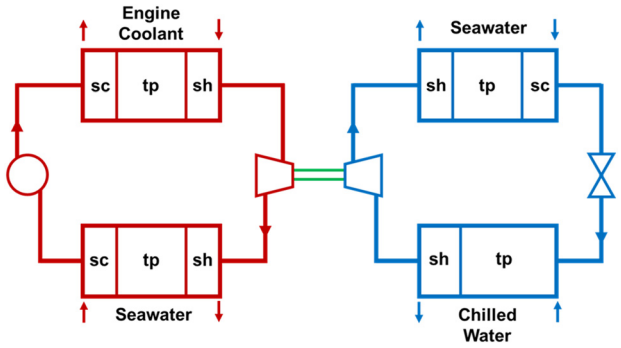

Fig. 3 Cycle diagram of the TCCS with each heat exchanger divided into regions based on working fluid phase. The subscripts "sc," "tp," and "sh" represent subcooled, two-phase, and superheated, respectively.

turbocompressor was chosen based on a recent study for a turbocompression cooling system [35]. In addition, the chilled water temperature difference (12–7 °C) was set based on commercially available chilled water delivery systems.

This study developed a detailed thermodynamic, heat exchanger, and economic simulation of a TCCS. An overview of the simulation approach is shown in Fig. 2. The thermodynamic model used the inputs from Table 1 to determine the state points, COP, and the turbomachinery power, size, and speed. The heat exchanger modeling used the state points and mass flows to determine overall heat transfer coefficients for the heat exchangers. Then, the heat exchanger area for each region was calculated using the ε-NTU method. After this, the total cost of the system was calculated using cost models for the major pieces of equipment and the refrigerant charge. Finally, the payback period was calculated based on how much power the turbocompression cooling system can displace from the diesel generators. The power displacement results in reduced fuel consumption and cost savings. The model was optimized by varying the effectiveness of the heat exchangers to minimize the payback period. This procedure was repeated with five different working fluids to determine how fluid parameters influence the COP, heat exchanger size, and payback period. The following sections will describe in greater detail the coupled thermodynamic, heat exchanger, and economic model.

2.1 Thermodynamic Model. A set of thermodynamic equations was solved in Engineering Equation Solver to understand the performance of the power cycle (organic Rankine cycle) and the cooling cycle (vapor compression cycle) [36]. The model assumed the turbocompression cooling system operated at steady-state and the system piping was well insulated. The throttling valve on the vapor compression cycle was assumed to be isenthalpic. In this work, each of the heat exchangers transferred energy between the working fluid refrigerant and a stream of single phase liquid. In the boiler, hot engine coolant, assumed to be water in the model, vaporized the working fluid. The condensers on the power and cooling cycles used seawater to cool the working fluid. In the chiller, the working fluid was vaporized to provide a cooling effect for a water stream.

The heat exchangers were divided into regions based on the phase of the working fluid: subcooled liquid, two-phase, and superheated vapor, as shown in Fig. 3. The condensing heat exchangers and the boiler (power cycle evaporator) were divided into liquid, two-phase, and superheated regions. The chiller (cooling cycle evaporator) was divided into two regions, two-phase and superheated, because the working fluid enters the chiller as a two-phase mixture after expansion through the throttling valve. Representative temperature-entropy diagrams for the cooling and power cycles are provided in Fig. 4. In the T-s diagram, the temperature profiles of the water streams (engine coolant, condensing water, and chilled water) are shown. On the vapor compression cycle, 1–2 represents the compression of the superheated working fluid. 2–3 is the cooling of the working fluid to a liquid phase through the condenser. 3–4 is the expansion of the working fluid through the throttling valve. From 4 to 1, the working fluid is vaporized to provide the desired cooling effect. On the power cycle, 1–2 is the pumping of the liquid working fluid to a higher pressure. From 2 to 3, the working fluid is vaporized by the waste heat from the engine coolant. From 3 to 4, the working fluid is expanded through the turbine to produce power for the compressor. Finally, from 4 to 1, the working fluid is condensed and cooled to the liquid phase.

The thermodynamic model used fundamental energy balances and heat exchanger design equations to calculate the state points throughout the organic Rankine cycle (power cycle) and the vapor compression cycle (cooling cycle). The energy transferred to the water stream of the heat exchangers was calculated with the following equation:

$$\dot{Q} = \dot{m}_{\mathrm{w}} c_{\mathrm{p}} (T_{\mathrm{w,i}} - T_{\mathrm{w,o}}) \tag{1}$$

where $\dot{m}_{\mathrm{w}}$ represents the mass flow rate of water, c_{p} represents the specific heat capacity of the water stream, and $T_{\mathrm{w,i}}$ and $T_{\mathrm{w,o}}$ represent the inlet and outlet temperatures of the water, respectively. The enthalpy change of the working fluid is defined in the following equation:

$$\dot{Q} = \dot{m}_{\mathrm{r}} (i_{\mathrm{i}} - i_{\mathrm{o}}) \tag{2}$$

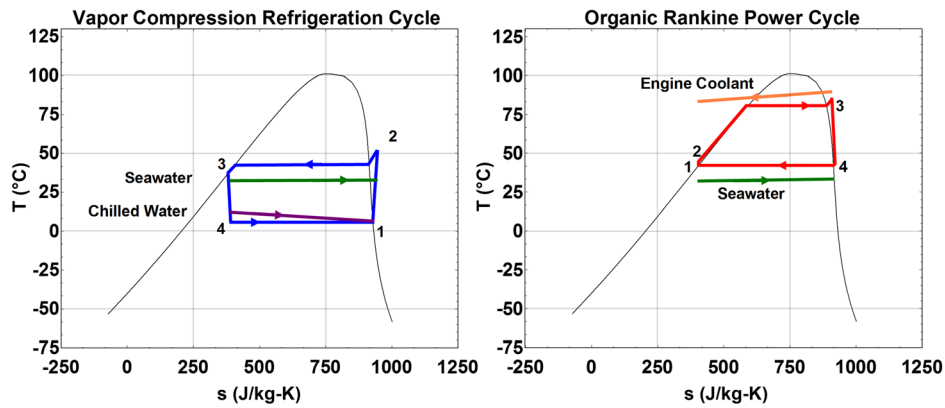

Fig. 4 Representative T-s diagrams for the (*a*) vapor compression refrigeration cycle and (*b*) organic Rankine power cycle where both use R134a. The engine coolant water flow, cooling seawater flow, and chilled water flow are overlaid.

where $\dot{m}$ represents the mass flow rate of the refrigerant working fluid, and i_i and i_o are the enthalpies of the working fluid at the inlet and the outlet. The heat exchanger design equation used to define the heat duty of a heat exchanger is given in the following equation:

$$\dot{Q} = \varepsilon C_{\min}(T_{h,i} - T_{c,i}) \tag{3}$$

where ε is the effectiveness of the heat exchanger, $C_{\min}$ is the minimum heat capacity rate between the water or refrigerant stream, and $T_{h,i}$ and $T_{c,i}$ represent the inlet temperatures of the hot and cold fluids, respectively. The set of Eqs. (1)–(3) was solved for each region of the heat exchangers, as shown in Fig. 3.The turbine, pump, and compressor were modeled with energy balance and isentropic efficiency equations. The isentropic efficiency of the turbine is defined in the following equation:

$$\eta_s = \frac{i_i - i_o}{i_i - i_{o,s}} \tag{4}$$

where η_s is the isentropic efficiency of the turbine and $i_{o,s}$ is the isentropic enthalpy at the turbine outlet. Eq. (5) was used to calculate the power output of the turbine

$$\dot{W}_{\text{turbine}} = \dot{m}_r(i_i - i_o) \tag{5}$$

The isentropic efficiencies of the pump and the compressor were calculated with the following equation:

$$\eta_s = \frac{i_{o,s} - i_i}{i_o - i_i} \tag{6}$$

Equation (7) defines the power output of the pump and compressor

$$\dot{W} = \dot{m}_r(i_o - i_i) \tag{7}$$

Equations (1)–(7) were solved simultaneously in Engineering Equation Solver to calculate the state points, refrigerant mass flow rates, and the heat duties of the heat exchangers in the power and cooling cycles.

Highly efficient turbomachinery is an essential component for the turbocompression cooling system. The efficiency of a turbocompressor depends primarily on the size and speed of the machine. The size and speed of rotating machinery can be determined with a Cordier analysis. The Cordier analysis used specific speed, specific diameter, volumetric flow rate, and the adiabatic head to calculate actual diameter and rotational speed of a turbine and compressor. Cordier maps have been empirically generated that show contours efficiency for typical devices, which depend on specific speed and specific diameter. The Cordier maps used in this study were generated by Barber-Nichols, Inc. for a wide range of specific speeds and diameters for both pumping and expanding machines [37]. In general, the specific speed of the turbine must be between 50 and 150, while the specific speed of the compressor must be between 60 and 200 to reach 80% isentropic efficiency. The specific speed, *Ns*, has units of $\text{ft}^{3/4}\ \text{lbm}^{3/4}\ \text{min}^{-1}\ \text{s}^{-1/2}\ \text{lbf}^{-3/4}$, while specific diameter, *Ds*, is in units $\text{lbf}^{1/4}\ \text{s}^{1/2}\ \text{lbm}^{-1/4}\ \text{ft}^{-1/4}$. The Cordier maps used in this work require the use of Imperial units for the specific speed and diameter. The specific speed and the specific diameter of a turbine and compressor are defined in the following equations:

$$Ns = \frac{N\sqrt{\dot{V}}}{(H_{ad})^{3/4}} \tag{8}$$

$$Ds = \frac{D(H_{ad})^{1/4}}{\sqrt{\dot{V}}} \tag{9}$$

where N is the actual speed of the rotating machinery in rev min^{-1}, V is the volumetric flow rate in $\text{ft}^3\ \text{s}^{-1}$, H_{ad} is the adiabatic head in ft lbf lbm^{-1}, and D is the diameter of the machine in feet. An important distinction in Eqs. (8) and (9) is that the specific speed and specific diameter are not dimensionless. The Cordier maps used in this study were developed using dimensional specific speed and diameter and have been shown elsewhere [35,37,38].

In each working fluid case, the specific speed of the turbine was set to 115, a value comfortably within the 80% island. From Eq. (8), the shaft rotational speed of the turbine was calculated. Then, the equation of the line that borders the 80% efficiency island on the Cordier map for the turbine was used to relate specific speed and specific diameter, which is defined in the following equation:

$$Ds_{\text{turbine}} = 2\left(\frac{Ns_{\text{turbine}}}{50}\right)^{-0.515} \tag{10}$$

Then, the actual diameter of the turbine was calculated using Eq. (9). The turbine and the compressor share the same shaft, so they spin at the same speed. The actual shaft speed was used in Eq. (8) to calculate the specific speed of the compressor. The equation of the line that borders the 80% isentropic efficiency island for the compressor was used to calculate the specific speed from the specific diameter, as shown in the following equation:

$$Ds_{\text{compressor}} = 1.75\left(\frac{Ns_{\text{compressor}}}{80}\right)^{-0.3802} \tag{11}$$

Then, Eq. (9) was used to calculate the diameter of the compressor.

The COP of the turbocompression cooling system was calculated using the below equation:

$$\text{COP} = \frac{\dot{Q}_{\text{chiller}}}{\dot{Q}_{\text{boiler}} + \dot{W}_{\text{pump}}} \tag{12}$$

Using Eqs. (1)–(12), the COP, state points, and mass flow rates of the turbocompression cooling system were calculated along with the size, speed, and power output of the turbomachinery. The state points and mass flow rates were input to the heat exchanger model to determine the size and pressure drop of the heat exchangers.

2.2 Heat Exchanger Model. The heat exchangers in this study were compact, gasketed plate and frame heat exchangers (PHX). There are a number of favorable characteristics of PHX for use in this specific application: small footprint, scalability, and flexibility. Smaller footprint is important in a shipboard cooling application as there is only a limited amount of free space available. The plate heat exchanger also has a much higher useful heat transfer area per volume when compared to shell and tube heat exchangers. Furthermore, the heat duty of the device can be easily scaled by adding or removing plates. In addition, these heat exchangers can be tailored specifically to certain applications. For example, the condenser plates in this study were designed to be manufactured from titanium to prevent corrosion from the seawater. The gasket material can be changed to account for working fluid compatibility and pressure rating considerations. There are a few limitations of gasketed plate heat exchangers compared to traditional shell and tube devices: lower operating temperature and pressure limits due to gasket material limits and higher pressure drop due to small flow channels [39,40]. The temperatures and pressures in this study were below the operational limits.

The geometric parameters for gasketed plate and frame heat exchanger in the present study were estimated from quotes and drawings received from manufacturers. The height and the width of the plate were 1.32 m and 1.17 m, respectively. The plate spacing was 0.0045 m and the thickness of the plates was 0.0007 m.

The plate spacing was calculated from the manufacturer quote based on the number of plates and relevant dimensions of the drawing. The chevron angle was not provided by the manufacturer quote, but was assumed to be 60 deg. The diameter of the inlet and outlet headers on the gasketed plate and frame heat exchanger was 0.350 m, while the length of the header depended on the number of plates.

The heat exchanger model calculated the total heat transfer area and the total pressure drop for each heat exchanger in the turbo-compression cooling system. The epsilon-NTU method was used to calculate the area of each region of the heat exchangers [41]. The number of transfer units was calculated from the effectiveness of the heat exchanger region, defined in Eq. (13) for a counter flow heat exchanger

$$\mathrm{NTU} = \frac{1}{\mathrm{Cr} - 1} \ln\left(\frac{\varepsilon - 1}{\varepsilon \mathrm{Cr} - 1}\right) \tag{13}$$

where Cr is the ratio of heat capacity rates between the water and refrigerant streams. The condensers and the boiler were modeled as counter flow devices. The relationship between the number of transfer units and effectiveness for a parallel flow heat exchanger is defined in the following equation:

$$\mathrm{NTU} = -\frac{\ln(1 - \varepsilon[1 + \mathrm{Cr}])}{1 + \mathrm{Cr}} \tag{14}$$

The cooling cycle chiller was modeled as a parallel flow heat exchanger. In this study, there was no difference between the chiller being modeled as a counter flow or parallel flow device because the majority of the heat transfer occurs in the phase change process. In some cases, a counterflow heat exchanger could increase superheat at the outlet of the chiller, which increases the compressor work and reduces cooling cycle COP. However, this would have limited impact in this work because the effectiveness in the superheated region of the chiller was 0.001. From the overall heat transfer coefficient and the number of transfer units, the heat exchange area was calculated based on the following equation:

$$\mathrm{NTU} = \frac{UA_{\mathrm{total}}}{C_{\mathrm{min}}} \tag{15}$$

where U is the overall heat transfer coefficient, A_{total} is the total heat exchanger area, and C_{min} is the minimum heat capacity rate. Equation (15) was used to calculate the heat exchange area for each region (subcooled, two-phase, and superheated) of every heat exchanger. The sum of the heat transfer areas of each region is the total heat exchange area, A_{total}, for a single heat exchanger.

Figure 5 shows a schematic of a single plate in the power cycle boiler. The plates are connected in parallel and each working fluid phase occupies a certain area of every plate. Once the total heat exchange area was determined, the number of plates for the plate and frame heat exchanger was calculated based on the dimensions of the plates, as shown in the following equation:

$$A_{\mathrm{total}} = A_{\mathrm{plate}}(N_{\mathrm{plate}} - 1) = w_{\mathrm{plate}}(L_{\mathrm{sc}} + L_{\mathrm{tp}} + L_{\mathrm{sh}})(N_{\mathrm{plate}} - 1) \tag{16}$$

Equation (16) approximates the heat transfer area of the plate heat exchanger which is consistent with methods available in the literature to determine heat transfer coefficients [42].

To calculate the heat transfer area, the overall heat transfer coefficient must be calculated, which is as follows:

$$\frac{1}{U} = \frac{1}{h_{\mathrm{r}}} + R_{\mathrm{wall}} + \frac{1}{h_{\mathrm{w}}} \tag{17}$$

U is the overall heat transfer coefficient, h_{r} and h_{w} are the heat transfer coefficients of the refrigerant and water side, respectively,

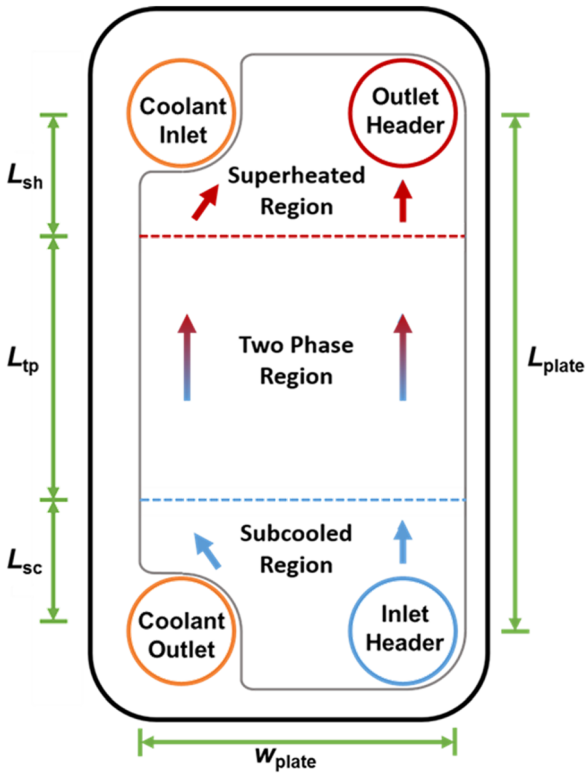

Fig. 5 Flow path and working fluid regions for a single plate in the power cycle boiling heat exchanger

and R_{wall} is the wall resistance of the plate. To calculate the overall heat transfer coefficient (and total heat transfer area), it was necessary to calculate the heat transfer coefficient in each region of the heat exchangers for the refrigerant and water flows.

There are a number of empirical heat transfer coefficient and pressure drop correlations for gasketed plate and frame heat exchangers available in the literature. The Kuo et al. correlation for condensing R-410a in plate heat exchangers was used for the two-phase regions of the condensers on the power cycle and cooling cycle [43]. The Kuo et al. correlation is defined in the following equation:

$$h_{\mathrm{r,cond}} = h_{\mathrm{r,l}}\left[0.25\mathrm{Co}^{-0.45}\mathrm{Fr}_{\mathrm{l}}^{0.25} + 75\mathrm{Bo}^{0.75}\right] \tag{18}$$

where $h_{\mathrm{r,l}}$ is the all liquid heat transfer coefficient in a plate heat exchanger, Co is the convection number, Fr_{l} is the liquid Froude number, and Bo is the boiling number. The all liquid heat transfer coefficient, $h_{\mathrm{r,l}}$, is defined according to the following equation:

$$h_{\mathrm{r,l}} = 0.2092\left(\frac{k_l}{D_{\mathrm{hyd}}}\right)\mathrm{Re}_{\mathrm{l}}^{0.78}\mathrm{Pr}_{\mathrm{l}}^{1/3}\left(\frac{\mu_{\mathrm{ave}}}{\mu_{\mathrm{wall}}}\right)^{0.14} \tag{19}$$

The dimensionless numbers used in this correlation are defined in the Nomenclature section of this paper. The Hsieh and Lin correlation for boiling R-410a in plate heat exchangers was used for the two-phase regions in the boiler and chiller [44], as shown in the following equation:

$$h_{\mathrm{r,boil}} = h_{\mathrm{r,l}}(88\mathrm{Bo}^{0.5}) \tag{20}$$

The simulation sensitivity to different correlations for heat transfer coefficients in plate heat exchangers will be examined in future studies. The heat transfer coefficient of the single phase regions in the heat exchangers was determined with the Thonon et al. correlation [45], defined in the following equation:

$$h_{sp} = 0.2298\mathrm{Re}^{0.645}\mathrm{Pr}^{1/3}\frac{k}{D_{hyd}} \tag{21}$$

The Thonon et al. correlation is valid for Reynolds numbers in the range of 50–15,000. The Reynolds number in the superheated regions was set to 15,000 which is the upper limit of the Thonon et al. correlation. After an extensive search through the literature, it was found that Reynolds number in PHX rarely exceeds 15,000–20,000 [46–50]. If the Reynolds number in these regions were not set, they would converge to values higher than 15,000. This produced unrealistically high heat transfer coefficients, which generated extremely small (and unrealistic) heat exchange area. The extremely small heat exchanger area would further compound the high Reynolds number and a recursive problem was encountered. Setting the Reynolds number to 15,000 avoided this problem and produced realistic values for single phase heat transfer coefficient.

In all of the cases, the water side (i.e., engine coolant, seawater, and chilled water) of the heat exchangers was single phase and turbulent, so the Dittus-Boelter correlation was used to calculate the heat transfer coefficient [41], as shown in the following equation:

$$h_w = 0.023\mathrm{Re}^{0.8}\mathrm{Pr}^{0.4}\frac{k_l}{D_{hyd}} \tag{22}$$

Figure 6 provides a schematic of the power cycle boiler plate frame heat exchanger, showing the refrigerant side inlet and outlet headers and four refrigerant channels that represent plates. The refrigerant enters the device in the bottom header and distributes into the plate arrangement. It was assumed that the flow was well distributed so each plate had an equal part of the total mass flow rate. As the refrigerant is heated, it travels up the plates and enters the two-phase flow regime. Once adequately heated, the superheated vapor flow recombines in the return header and flows to the turbine. The pressure drop of the refrigerant flow was calculated in the headers and the plate channels.

The pressure drop in the two-phase regions of the heat exchangers was calculated using the Kuo et al. and Hsieh and Lin correlations for friction factors of condensing and boiling refrigerants.

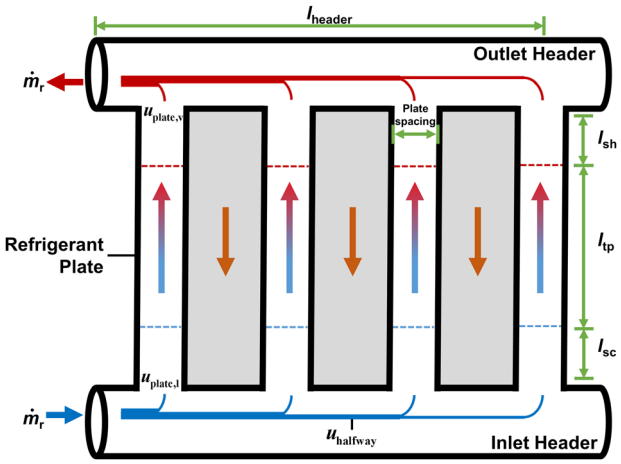

Fig. 6 Cross section of the flow path in the power cycle boiler with four refrigerant channels. The pressure drop through the single phase regions is the sum of major losses and minor losses. The minor losses are due to flow branching into the plates and the sudden contraction/expansion, while major losses are due to friction in the header and in the refrigerant channels. The gray regions represent flow area of hot engine coolant.

The Kuo et al. friction factor was calculated with the following equation:

$$f_{tp,cond} = 21500\mathrm{Re}_{eq}^{-1.14}\mathrm{Bo}^{-0.085} \tag{23}$$

where Re_{eq} is the equivalent Reynolds number. The Hsieh and Lin friction factor is defined by the below equation:

$$f_{tp,boil} = 61,000\mathrm{Re}_{eq}^{-1.25} \tag{24}$$

The pressure drop in the two-phase regions was calculated with the following equation:

$$\Delta P_{tp} = \frac{2f_{tp}G^2}{\rho}\frac{L_{tp}}{D_{h,channel}} \tag{25}$$

where G is the refrigerant mass flux, L_{tp} is the area of the two-phase region divided by the width of the plate, and $D_{h,channel}$ is the hydraulic diameter of the flow channels. The pressure drop in the single phase refrigerant regions of the heat exchangers was calculated as the sum of the header pressure drop, minor losses from the bend and sudden contraction/expansion, and the major losses from the flow of the working fluid through the plate channels, as shown in the following equation:

$$\Delta P_{sp} = \Delta P_{header} + \Delta P_{tee} + \Delta P_{channel} \tag{26}$$

Since flow is branching into and out of the header, the velocity at each point along the length of the header was not constant, and, thus, the pressure drop varied. The slight pressure recovery due to the recombining flow in the return header was ignored. In addition, it was assumed that the effects of gravity were negligible because the system was a closed loop. To simplify this calculation, the velocity of the fluid stream through the pipe was calculated when half of the flow has branched into the plates, as shown in Fig. 6. This velocity was used through the length of the header to determine an approximate pressure drop, as shown in the following equation:

$$\Delta P_{header} = \frac{K_{tee,line}\rho u_{halfway}^2}{2} + \frac{2f_{fanning}\rho u^2 L_{header}}{D_{header}} \tag{27}$$

where $K_{tee,line}$ is the loss coefficient for the flow that remains in the header after a branch, $f_{fanning}$ is the Fanning friction factor, and L_{header} is the length of the header [51,52]. The length of the header is determined by the number of plates, plate thickness, and plate spacing. The pressure drop from the tee was calculated using the below equation:

$$\Delta P_{tee} = \frac{K_{tee,branch} + K_{con/exp}\rho u_{channel}^2}{2} \tag{28}$$

where $K_{tee,branch}$ is the loss coefficient for flow that branches out of the header and $K_{con/exp}$ is the loss coefficient due to a sudden contraction or expansion [40,41]. The inlet headers use the sudden contraction loss coefficient, while outlet headers use sudden expansion loss coefficient. The velocity of the refrigerant in the channels between the plates was calculated using the below equation:

$$\Delta P_{header} = \frac{\dot{m}_r}{0.5N_{plates}}\frac{1}{\rho}A_c \tag{29}$$

where A_c is the cross-sectional area of the refrigerant flow. A_c is the equal to the spacing between the plates multiplied by the width of the plates, as shown in Figs. 5 and 6. The pressure drop through the plate was calculated according to the following equation:

$$\Delta P_{\text{channel}} = \frac{2 f_{\text{thonon}} \rho u_{\text{channel}}^2 L_{\text{sp}}}{D_{\text{h,channel}}} \tag{30}$$

where L_{sp} is the vertical length of the single phase region along the plates of the heat exchanger as shown in Fig. 6. The sum of the liquid and vapor phase refrigerant pressure drop through the heat exchangers and headers was multiple orders of magnitude smaller than the pressure drop through the two-phase region. The pressure drop through the plates was significantly higher than the pressure drop through the headers, which confirms that the flow was well distributed in the plates. In general, the total pressure drop of the refrigerant side in the heat exchangers had a minimal effect on the COP and the payback period of the total system.

2.3 Economic Model. The cost of the heat exchangers, refrigerant, turbocompressor, power cycle pump, and piping and fittings were calculated in the third block of the model. The cost model from Brown et al. was used for the plate heat exchangers [53], as defined in the following equation:

$$\text{cost}_{\text{HX}} = 1713.8 (A_{\text{total}})^{0.54} F_{\text{material}} F_{\text{pressure}} \frac{\text{CEPCI}_{2016}}{\text{CEPCI}_{2005}} \tag{31}$$

where A_{total} is the total area of the heat exchanger in m^2, F_{material} is a cost multiplier based on the plate material, F_{pressure} is a cost multiplier based on the operating pressure of the device, and CEPCI is the Chemical Engineering Plant Cost Index used to update the cost model to present day [54]. F_{material} is equal to 1 for stainless steel plates and 1.6 for titanium plates. F_{pressure} is equal to 1.23 for operating pressures above 1620 kPa and 1.35 for pressures above 2551 kPa.

The amount of refrigerant charge in the system was calculated by determining the volume of the heat exchangers and piping. In each region of the system, the volume was multiplied by the fluid density to determine the mass. In the two-phase regions of the heat exchangers, an average density based on saturated liquid and saturated vapor was used. The diameter of piping was calculated by assuming a pressure drop through each run and setting a length. After setting these two values, minor loss equations were used to calculate the pressure drop. The length of the pipe was estimated with guidance from construction of an air coupled turbocompression cooling system [55]. After pipe diameter was determined, the volume could be calculated and thus the mass of refrigerant.

At the outlet of the throttling valve, the working fluid is a two-phase mixture flowing through a pipe run and into the chiller. The density in this section of pipe was calculated as a weighted average, based on quality, of saturated liquid and vapor densities, as shown in the following equation:

$$\rho_{\text{tp}} = x \rho_{\text{v}} + (1 - x) \rho_{\text{l}} \tag{32}$$

Then, with quotes from refrigerant suppliers, the total cost of the refrigerant charge was calculated.

The turbocompressor cost model was developed as a logarithmic fit between two data points obtained from a supplier that has designed and manufactured the turbomachine for the previous work on turbocompression cooling [35]. The cost model is a function of the delivered power of the turbine, in kW, as shown in the following equation:

$$\text{cost}_{\text{TC}} = \text{cost}_{6\text{kw}} \left(\frac{\dot{W}_{\text{turbine}}}{6} \right)^{0.3569} \tag{33}$$

The cost of the power cycle pump was estimated using the model from Couper et al. [56]. The pump was assumed to be a cast iron centrifugal pump, where the cost is defined in the following equation:

$$\text{cost}_{\text{pump}} = \text{cost}_{\text{base}} F_{\text{material}} F_{\text{type}} \frac{\text{CEPCI}_{2016}}{\text{CEPCI}_{1985}} \tag{34}$$

where $\text{cost}_{\text{base}}$ is the base cost of the machine, which depends on volumetric flow rate and head provided. F_{material} is a material cost multiplier, and F_{type} is a cost multiplier to account for the type of the machine, which depends on volumetric flow rate and head provided. The equations defining $\text{cost}_{\text{base}}$ and F_{type} can be found in Couper et al. [56].

The cost of the piping was determined with the cost model from Brown, which depends on diameter, length, and the number of fittings in the pipe run [53]. In this work, it was assumed that there would be one fitting per 1.80 m of piping. The cost of the system piping was determined from the following equation:

$$\text{cost}_{\text{pipe}} = (\text{Fitting} + 9.24) 3.281 L \left(\frac{D_{\text{pipe}}}{0.0254} \right)^{0.83} \tag{35}$$

where *Fitting* is the number of fittings per 30 m of piping (equal to 16.67), D_{pipe} is the diameter of the pipe, and L is the length of the pipe.

The fuel savings from the turbocompression cooling system were determined based on the cooling capacity, the COP of the current vapor compression chillers, the efficiency of the motor-generator interface, and the thermal efficiency of the diesel engine. The power displaced from the engines by implementation of a TCCS was calculated using the below equation:

$$\dot{W}_{\text{displaced}} = 0.85 \left(\frac{\dot{Q}_{\text{chiller}}}{COP_{VC}} - \dot{W}_{\text{pump}} \right) \tag{36}$$

The power displacement is multiplied by 0.85 to account for the time when the marine cargo vessel is cold ironing or receiving shore power. During cold ironing, the diesel generators are turned off and the ship is connected to the mainland electrical grid. The baseline COP of the vapor compression chillers onboard large cargo ships is nominally equal to 4. The amount of engine power offset by the TCCS was calculated in the following equation:

$$\dot{W}_{\text{engine}} = \frac{\dot{W}_{\text{pump}}}{\eta_{\text{gen}}} \tag{37}$$

Based on the thermal efficiency of the diesel engine, the heat input was calculated with the following equation:

$$\dot{Q}_{\text{engine}} = \frac{\dot{W}_{\text{engine}}}{\eta_{\text{thermal}}} \tag{38}$$

Finally, the amount of fuel saved was calculated with the following equation:

$$\dot{m}_{\text{MGO}} = \frac{\dot{Q}_{\text{engine}}}{Q_{\text{LHV,MGO}}} \tag{39}$$

The mass flow rate was converted to an annual basis and the simple payback period was determined with the following equation:

$$\text{Payback Period} = \frac{\text{cost}_{\text{TCCS}}}{\text{cost}_{\text{MGO}} \dot{m}_{\text{MGO}}} \tag{40}$$

Once the payback period was determined, the system was optimized based on heat exchanger effectiveness to find a minimum payback period.

2.4 Optimization Routine and Sensitivity Analysis. The coupled thermodynamic, heat exchanger, and economic model were optimized with a search and find method to minimize the

simple payback period. There are several parameters that can be altered to optimize the payback period of this system: closest approach temperatures, saturation pressures, or heat exchanger effectivenesses. In this work, the payback period of the waste heat recovery system was minimized by finding an optimum combination of heat exchanger effectivenesses. The effectiveness of the heat exchangers directly relates to the heat exchange area, which was the primary input for most heat exchanger cost models. The heat exchangers account for a significant fraction of the total system cost (~75%) which made the effectiveness an ideal optimization parameter.

After coupling the thermodynamic and heat transfer models and setting the Reynolds number to 15,000 in the superheated regions, only three effectiveness values were left as inputs to the model. The subcooled regions of the power and cooling cycle condensers ($\varepsilon_{PC,Csc}$ and $\varepsilon_{CC,Csc}$, respectively) and the superheated region of the cooling cycle chiller ($\varepsilon_{CC,Esh}$) were inputs. Setting the superheated Reynolds number in the heat exchangers fixed the effectiveness values in those regions. With these three effectiveness values input along with temperatures and mass flow rates of the external streams, the model calculated the effectiveness in every other region of the heat exchangers on both the power and cooling cycles. The simulation was manually optimized by varying these three heat exchanger effectiveness values until the payback period was minimized. The subcooled power cycle condenser effectiveness was optimized first, then the subcooled cooling cycle condenser effectiveness, and finally, the superheated cooling cycle evaporator. The manual optimization method was an effective technique for this study because the model is highly sensitive to small changes in effectiveness. The search and find routine was performed three times to ensure the effectiveness values converged to their optimum value with a minimized payback period. Other optimization methods are possible, but the search and find method guaranteed that the optimal system results were found.

In addition, a sensitivity analysis was performed on the heat exchanger effectivenesses. For the sensitivity study, the Reynolds number in the superheated regions was not set in order to examine more effectiveness values. In the sensitivity study, each effectiveness input was changed by 0.1 from its optimized value and the effect on payback period was noted. The results of the optimization and the sensitivity analysis will be presented in Sec. 3.

2.5 Working Fluid Selection. The choice of working fluid is critically important to the performance of both the power and cooling cycles. There are certain thermodynamic and physical characteristics of working fluids that make them particularly attractive for use in an ORC or a vapor compression cycle. The critical temperature and pressure must be sufficiently high to ensure that the critical point is never reached. Reaching the critical point could significantly change the physical, chemical, and heat transfer properties of the fluid. Investigating transcritical and supercritical turbocompression cooling systems is left to future studies.

The slope of the saturated vapor line on a temperature-entropy diagram is an important factor for organic Rankine cycles. If the working fluid has a negative slope, an isentropic expansion could drive the fluid into the two-phase region of the vapor dome. The formation of liquid droplets in the turbine during fluid expansion will cause serious damage and erosion of the turbine blades. A fluid with a negative slope, such as water, is called a wet working fluid. A fluid which has an infinite slope is called isentropic. This fluid is preferable to a wet working fluid, but a fluid that has a positive slope is the best candidate for an organic Rankine cycle. A dry working fluid (one with a positive slope) does not enter the vapor dome after it undergoes an isentropic expansion, which is ideal to preserve the integrity of the turbomachinery.

In addition, there are several safety factors that make certain fluids attractive for use in these cycles. As leaks are always present in real systems, the flammability, toxicity, and environmental factors should be considered when choosing a working fluid. The ozone depletion potential and the global warming potential (GWP) are two important characteristics to consider. There are many working fluids that have favorable thermodynamic properties, but can damage the ozone layer and contribute to global warming. The next generation of working fluids have lower GWP and favorable thermodynamic properties. This study examined five different working fluids: R134a, R245fa, R1234ze(E), R152a, and R600a, which are shown in Table 2. These working fluids have sufficiently high critical points along with isentropic or dry saturated vapor lines. R134a and R1234ze(E) were chosen in this study because they are used in state of the art commercially available vapor compression chillers [57–59]. R245fa is a commonly used fluid for low-grade waste heat recovery in organic Rankine cycles, while R152a was chosen based on guidance from a recently conducted experimental study on a turbocompression cooling system for low grade waste heat recovery [35,55,60]. R600a was chosen because of the favorable performance found in the literature for low-grade waste heat recovery in coupled organic Rankine-vapor compression systems [61–63]. The same working fluids are used on both sides of the cycle. Higher COP turbocompression cooling systems could be achieved by using different working fluids on the power and cooling cycle to optimize the performance of each side, but these are left to future studies.

3 Results and Discussion

The optimization routine described in Sec. 2.4 found the minimum payback period for each of the five working fluids examined. The breakdown of system cost for the optimized solution of each working fluid is given in Fig. 7. The heat exchangers, on average, make up over 78% of the total system cost. The payback period for each system is also given in Fig. 7, labeled as "PP." The TCCS with R152a had the lowest overall system cost, $181,846, because the heat exchangers were smaller than the other systems. There are two benefits to smaller heat exchangers: the heat exchangers will be cheaper and the amount of refrigerant charge in the devices will be lower. The highest total system cost was found with R245fa of $310,137. Along with the lowest initial investment cost, the turbocompression cooling system with R152a as a working fluid had the lowest simple payback period of 1.46 years (about 533 days) in the study. The COP of the optimized systems ranged from 0.269 for the R245fa case to 0.415 for the R1234ze(E) system. The high condensing seawater temperature in this study (32 °C) is one of the main causes of the low COP. This temperature was chosen to demonstrate the capabilities of the TCCS even in extreme cases. Large cargo ships spend a considerable amount of time in locations with seawater colder than 32 °C, which will significantly improve the performance of the TCCS.

Table 2 Characteristics of the working fluids chosen for this study. Every refrigerant in this study had an ozone depletion potential of zero.

Working fluid	GWP (100 yr)	Class	Type	Flammable	Toxic	T_{crit}/P_{crit} (°C)/(kPa)	Cost ($/kg)
R134a	1430	HFC	Isentropic	No	No	101/4059	11.00
R152a	124	HFC	Dry	Yes	No	113/4520	12.20
R245fa	1030	HFC	Dry	Yes	No	154/3651	41.40
R1234ze(E)	6	HFO	Isentropic	No	No	109/3632	33.00
R600a	3	Natural	Isentropic	Yes	No	135/3640	41.80

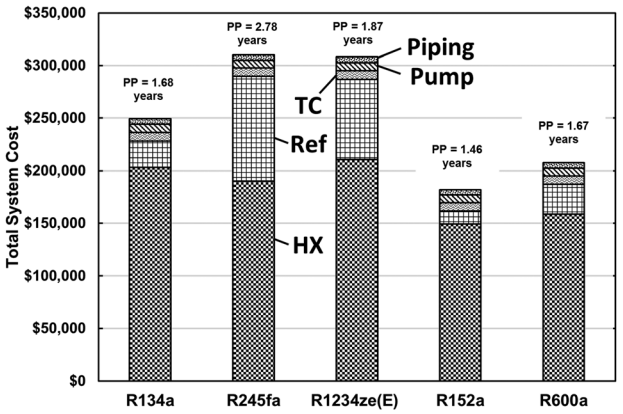

Fig. 7 Breakdown of system cost for each working fluid. Payback period is denoted as "PP."

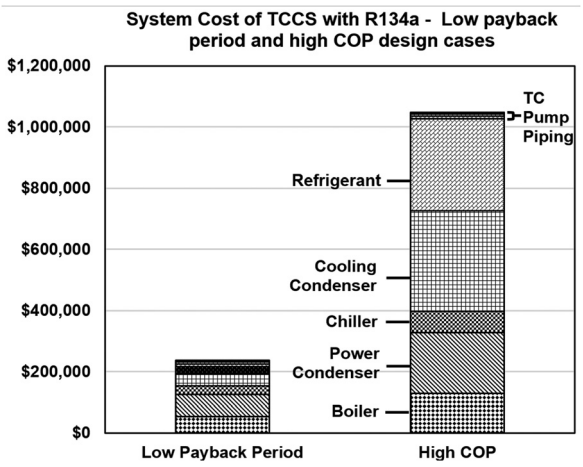

Fig. 9 Comparison of total system cost for the TCCS with R134a designed for energy efficiency and the system designed to have a minimum payback period. The high COP TCCS is 4.4 times more expensive than the low payback period system.

The other main cause of the low COPs found in this work was simply the optimization goal. The goal was to seek out the minimum payback period of the TCCS, which does not necessarily yield the most energy efficient system (highest COP). Figure 8 provides a T-s diagram of a turbocompression cooling system designed to have a higher COP. The COP of the higher efficiency case was 0.528, while the COP of the system optimized for payback period was 0.384. Increasing the COP from 0.384 to 0.528 increased the annual savings by just under $61,931. A comparison of the costs for the energy-optimized system and the payback period optimized system is shown in Fig. 9. The total cost of the performance optimized system was $1.48 million, about 5.9 times higher than the payback period optimized system which was $249,254. The individual component with the most dramatic cost increase was the refrigerant charge, which increased from $24,787 (about 10% of the total system cost) to $497,286 (34% of the total system cost). The amount of refrigerant in the system increased so dramatically because the total area of the heat exchangers increased from 863 m^2 to 15,494 m^2. With the increase in heat exchange area also came an increase in cost of the four heat exchangers, from $203,155 (82% of the total system cost) to $959,952 (65% of the total system cost). The heat exchanger fraction of total system cost decreased because the refrigerant occupied a larger fraction of the cost. The cooling cycle condenser was 9.1 times more expensive, while the power cycle condenser was 4.2 times more expensive on the performance optimized system.

From these results, it is obvious that the most energetically efficient system is not necessarily the most economically viable option. It is critically important to weigh the actual cost of the components against the energetic performance and annual savings to determine a realistic system design. If both systems operated for a period of 10 years, the payback period optimized system would save $610,320 more than the high efficiency system.

The characteristics of the plate and frame heat exchangers for the R152a system can be seen in Table 3, which include the effectiveness of each region, number of plates, pressure drop, and cost. The optimization routine sought to increase the amount of superheat from the boiler and decrease the superheat leaving the chiller. More superheat from the boiling heat exchanger will increase the enthalpy of the working fluid at the turbine inlet which should yield a higher turbine power output. Reducing the superheat at the chiller outlet will reduce the amount of energy the cooling cycle condenser needs to reject, reducing the size of the cooling cycle heat exchangers. The condensing heat exchangers were made from titanium which made them the most expensive heat exchangers on their respective power and cooling cycles, so the optimization routine sought to keep the effectiveness values in these heat exchangers lower. The pressure drop through the heat exchangers was small enough that it did not have a significant impact on the model outputs.

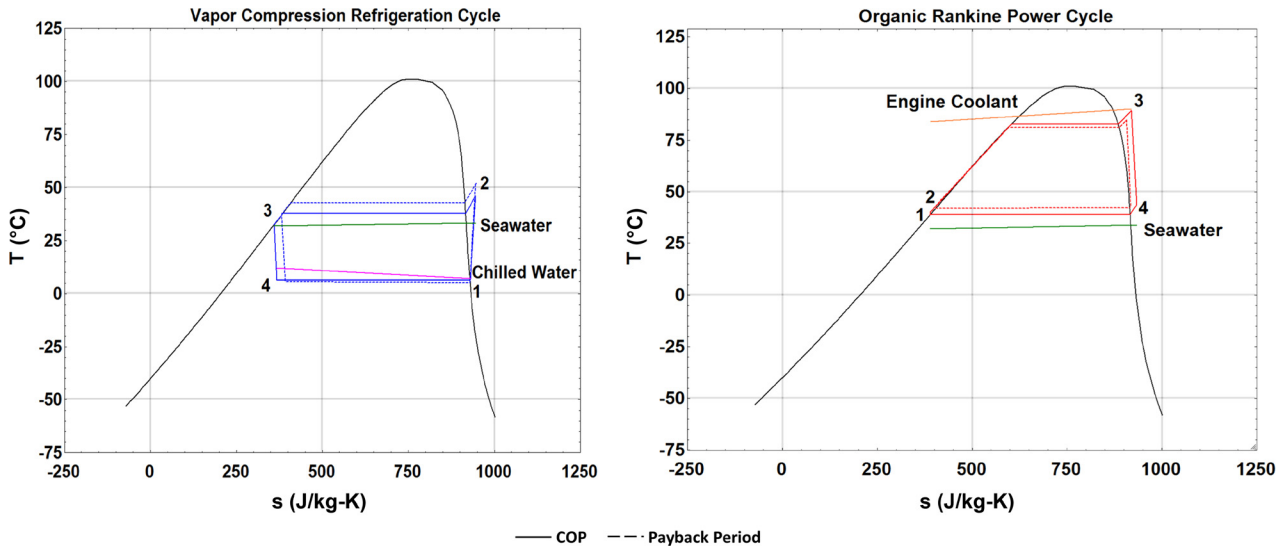

Fig. 8 T-s diagrams for a turbocompression cooling system with working fluid R134a designed to have a higher COP

Table 3 The optimized effectiveness values, number of plates, pressure drop, and cost of the heat exchangers for the R152a system

Cycle	Heat exchanger	Effectiveness	Plates	ΔP	Cost
Power cycle	Boiler: subcooled	0.660	123	0.80 kPa	$34,053
	Boiler: two-phase	0.280			
	Boiler: superheated	0.843			
	Condenser: superheated	0.482	141	4.30 kPa	$58,737
	Condenser: two-phase	0.139			
	Condenser: subcooled	0.001			
Cooling cycle	Chiller: two-phase	0.743	63	5.40 kPa	$23,511
	Chiller: superheated	0.001			
	Condenser: superheated	0.576	49	4.00 kPa	$33,013
	Condenser: two-phase	0.053			
	Condenser: subcooled	0.460			

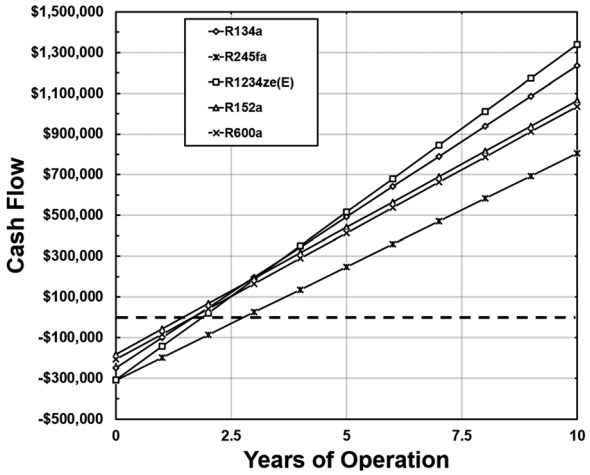

Fig. 10 Cash flow after implementation of the TCCS over a 10-year period

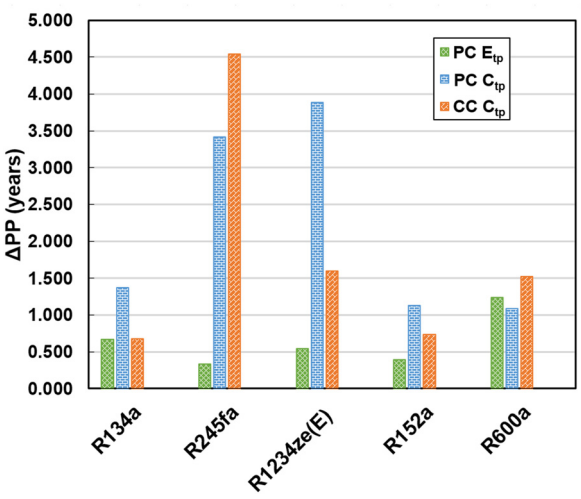

Fig. 11 Change in payback period as a function of changing heat exchanger effectiveness in the designated regions by 0.1. The three effectiveness regions with the greatest impact on payback period are shown.

Figure 10 provides a cash flow over a 10 year period of operation for the TCCS applied to a marine diesel generator set. The simple cash flow diagram starts in the negative region of the plot due to the initial capital investment. Since the turbocompression cooling system reduced fuel expenditures each year, the cash flow curve rose linearly and eventually crossed the red dotted lin which represents the payback period. With an operational life time of 10 years, the R1234ze(E) system saved the most money at $1,399,666. The R1234ze(E) system saved the most money because it had a high system COP at 0.415, saving $164,775 per year.

In addition to calculating the payback period of the five systems, a sensitivity analysis was performed to determine which effectiveness values had the greatest impact on payback period. The results of the sensitivity study are provided in Fig. 11. For every working fluid, the effectiveness value of each heat exchanger region was changed by 0.1 and the change in payback period was noted. The three heat exchanger regions with the greatest impact on payback period are shown in Fig. 11 for each working fluid. "CC" and "PC" represent cooling cycle and power cycle heat exchangers, respectively, while "E" and "C" represent evaporator or condenser. "TP" represents the two-phase region of the heat exchanger. For example, PC C_{tp} represents the impact of the effectiveness in the two-phase region of the power cycle condenser. In every case, the two-phase regions of the condensers on the cooling and power cycles had the largest impact on payback period because they were the most expensive heat exchangers. The two-phase region was specifically impactful because over 95% of the total heat duty of the heat exchangers was exchanged in these regions. Finding the most ideal area for the condensing heat exchangers was critical to finding the minimum payback period of the turbocompression cooling cycle.

As seen in Fig. 11, the cooling and power cycle condenser effectiveness values in the turbocompression cooling system with R245fa had the largest impact on payback period throughout all the test cases. Of the fluids examined, R245fa had the highest saturation temperature and a low slope of the saturated liquid line on a pressure-enthalpy diagram. Due to the low slope of the saturated liquid line, small increases in condenser pressure can greatly increase the chiller inlet quality. The increase in chiller quality will decrease the amount of cooling the chiller can provide, lowering the overall COP. Small changes in effectiveness will affect the condenser pressure which has a profound impact on the cooling duty and COP of the R245fa system.

A summary of thermodynamic characteristics of the turbocompression cooling systems in this study is provided in Table 4. The TCCS with R1234ze(E) had the highest overall COP of 0.415 with a cooling capacity of 837 kW. The R134a system had highest organic Rankine cycle thermal efficiency at 8.1%, while R1234ze(E) system had the highest vapor compression cycle COP of 5.58. Some of the working fluids had higher vapor compression COPs and low ORC thermal efficiency, while others had high ORC thermal efficiency and low vapor compression COPs. There may be an optimal combination of working fluids that can simultaneously maximize the cooling cycle COP and the thermal efficiency of the power cycle. An important consideration for a combination of fluids is to have matching size and speed for the turbomachinery. Examining combinations of working fluids will be part of a future study.

Table 4 Comparison of each TCCS with different working fluids

Working fluid	System COP	$\dot{Q}_{chill}$ (kW)	$\dot{W}_{turb}$ (kW)	$\dot{W}_{comp}$ (kW)	η_{ORC}	COP_{VC}	TC speed (rpm)	D_{turb} (m)	D_{comp} (m)
R134a	0.384	775	161	153	0.081	5.06	27,887	0.125	0.164
R152a	0.311	626	133	127	0.066	4.93	33,803	0.121	0.149
R245fa	0.269	539	133	126	0.066	4.27	16,288	0.212	0.302
R1234ze(E)	0.415	837	158	150	0.079	5.58	23,658	0.144	0.194
R600a	0.305	613	129	123	0.064	5.00	30,959	0.147	0.185

The specific speed of the turbine was set to 115 to compare the size and speed of the turbomachinery for various working fluids as shown in Table 4. The turbocompressor in the TCCS with R245fa had the largest diameter and the lowest rotational speed because the volumetric flow rate through the turbine was the highest of all the working fluids. Low density at the turbine outlet and high mass flow rate for the R245fa system contribute to the high volumetric flow rate, and thus, large turbomachine diameter.

4 Conclusion

The present study examined five different working fluids for use in a turbocompression cooling system driven by low grade waste heat in the engine coolant of a large marine diesel generator set. The system model was optimized by altering the effectiveness of the heat exchangers to find the minimum payback period. The TCCS with R152a had the lowest payback period of 1.46 years with a cooling capacity of 626 kW. Over a 10 year period, the TCCS with working fluid R1234ze(E) had the largest payout of $1,399,666. This work found that minimizing exergy destruction or maximizing COP may not yield the most economical system due to significant increases in component costs without providing a major increase in annual savings. Therefore, it is important to take into account actual system costs when performing a technoeconomic study on waste heat recovery systems.

There are several aspects of this work that require further investigation. In a future study, more working fluids and combinations of working fluids will be studied. The cooling cycle and power cycle can use different working fluids to maximize the efficiency of both cycles. In this work, if R1234ze(E) was used on the cooling cycle and R134a on the power cycle, a better overall system performance could have been realized. In addition, investigation into various waste heat scenarios, including diesel engine exhaust or gas turbine exhaust, would help to understand how waste heat phase, temperature, and flow rate affect the technoeconomic performance of the turbocompression cooling system. In addition to different waste heat scenarios, examining the performance of the system at different ambient conditions is an important consideration to understand how condensing temperature will affect system performance. Future studies will also investigate the effects of adding recuperating heat exchangers. Incorporating these additional heat exchangers should significantly improve the performance of the system and decrease the payback period.

Acknowledgment

The authors would like to thank Barber-Nichols, Inc. for their insight on turbocompressor cost and modeling inputs, specifically Jeff Shull, Robert Fuller, and Jeff Noall.

Funding Data

- The Department of Energy Advanced Research Project Agency-Energy (ARPA-e) (Contract No. DE-AR0000574).

Nomenclature

Variable Description Units/Formula

A = area (m^2)
Bo = boiling number, $Bo = q''/Gi_{fg} = A_c/A_{plate}$
C = heat capacity rate ($W\ K^{-1}$)
c_p = specific heat capacity ($J\ kg^{-1}\ K^{-1}$)
Co = convection number, $Co = (\rho_g/\rho_l)((1-x)/x)^{0.8}$
Cr = heat capacity rate ratio
CEPCI = Chemical Engineering Plant Cost Index
COP = coefficient of performance
D = diameter, m (or ft)
Ds = dimensional specific diameter ($lbf^{1/4}\ s^{1/2}\ lbm^{-1/4}\ ft^{-1/4}$)
f = friction factor
F = cost multiplying factor
Fr = Froude number, $Fr = G^2/(\rho^2 g D_{hyd})$
g = acceleration from gravity ($m\ s^{-2}$)
G = mass flux ($kg\ m^{-2}\ s^{-1}$)
h = heat transfer coefficient ($W\ m^{-2}\ K^{-1}$)
H = head rise ($ft\ lbf\ lbm^{-1}$)
i = enthalpy ($W\ kg^{-1}$)
i_{fg} = enthalpy of vaporization (J)
k = thermal conductivity ($W\ m^{-1}\ K^{-1}$)
K = loss coefficient
L = length (m)
$\dot{m}$ = mass flow rate ($kg\ s^{-1}$)
N = rotational speed ($rev\ min^{-1}$)
N_{plate} = number of plates
Ns = dimensional specific speed ($ft^{3/4}\ lbm^{3/4}\ min^{-1}\ s^{-1/2}\ lbf^{-3/4}$)
NTU = number of transfer units
P = wetted perimeter (m)
Pr = Prandtl number, $Pr = \mu c_p/k$
q'' = heat flux ($W\ m^{-2}$)
$\dot{Q}$ = heat transfer rate (W)
R_{wall} = wall thermal resistance ($m^2\ K\ W^{-1}$)
Re = Reynolds number, $Re = 4\dot{m}/P\mu$
T = temperature (°C)
u = velocity ($m\ s^{-1}$)
U = overall heat transfer coefficient ($W\ m^{-2}\ K^{-1}$)
V = volumetric flow rate ($ft^3\ s^{-1)}$
W = power (W)
w_{plate} = width of plates (m)
x = quality
ΔP = static pressure change (kPa)
ρ = density ($kg\ m^{-3}$)

Greek Symbols

ε = heat exchanger effectiveness
η = efficiency
μ = dynamic viscosity (kPa s)
ν = kinematic viscosity ($m^2\ s^{-1}$)

Subscripts and Superscripts

ad = adiabatic
boil = boiling
c = cold side
c = cross-sectional
CC = cooling cycle
cond = condensing
eq = equivalent
gen = generator
h = hot side
hyd = hydraulic
i = in

l = liquid
LHV = lower heating value
min = minimum
MGO = marine gas oil
o = out
PC = power cycle
r = refrigerant side
s = isentropic
sc = subcooled region
sh = superheated region
tp = two-phase region
VC = vapor compression
w = water side

References

[1] Little, A. B., and Garimella, S., 2011, "Comparative Assessment of Alternative Cycles for Waste Heat Recovery and Upgrade," Energy, **36**(7), pp. 4492–4504.
[2] Angelino, G., and Invernizzi, C., 2003, "Experimental Investigation on the Thermal Stability of Some New Zero ODP Refrigerants," Int. J. Refrig., **26**(1), pp. 51–58.
[3] Ito, M., Dang, C., and Hihara, E., 2014, "Thermal Decomposition of Lower-GWP Refrigerants," International Refrigeration and Air Conditioning Conference, West Lafayette, IN, July 14–17, p. 1538.
[4] Al-Tahaineh, H., Frihat, M., and Al-Rashdan, M., 2013, "Exergy Analysis of a Single-Effect Water-Lithium Bromide Absorption Chiller Powered by Waste Energy Source for Different Cooling Capacities," Energy Power, **3**(6), pp. 106–118.
[5] Manu, S., and Chandrashekar, T. K., 2016, "A Simulation Study on Performance Evaluation of Single-Stage LiBr–H_2O Vapor Absorption Heat Pump for Chip Cooling," Int. J. Sustainable Built Environ., **5**(2), pp. 370–386.
[6] de Vega, M., Almendros-Ibañez, J. A., and Ruiz, G., 2006, "Performance of a LiBr-Water Absorption Chiller Operating With Plate Heat Exchangers," Energy Convers. Manage, **47**(18–19), pp. 3393–3407.
[7] Jakob, U., Eicker, U., Schneider, D., Taki, A. H., and Cook, M. J., 2008, "Simulation and Experimental Investigation Into Diffusion Absorption Cooling Machines for Air-Conditioning Applications," Appl. Therm. Eng., **28**(10), pp. 1138–1150.
[8] González-Gil, A., Izquierdo, M., Marcos, J. D., and Palacios, E., 2011, "Experimental Evaluation of a Direct Air-Cooled Lithium Bromide-Water Absorption Prototype for Solar Air Conditioning," Appl. Therm. Eng., **31**(16), pp. 3358–3368.
[9] Ge, Y. T., Tassou, S. A., and Chaer, I., 2009, "Modelling and Performance Evaluation of a Low-Temperature Ammonia-Water Absorption Refrigeration System," Int. J. Low-Carbon Technol., **4**(2), pp. 68–77.
[10] Le Lostec, B., Galanis, N., and Millette, J., 2012, "Experimental Study of an Ammonia-Water Absorption Chiller," Int. J. Refrig., **35**(8), pp. 2275–2286.
[11] Ouadha, A., and El-Gotni, Y., 2013, "Integration of an Ammonia-Water Absorption Refrigeration System With a Marine Diesel Engine: A Thermodynamic Study," Procedia Comput. Sci., **19**, pp. 754–761.
[12] Chua, H. T., Ng, K. C., Malek, A., Kashiwagi, T., Akisawa, A., and Saha, B. B., 2001, "Multi-Bed Regenerative Adsorption Chiller - Improving the Utilization of Waste Heat and Reducing the Chilled Water Outlet Temperature Fluctuation," Int. J. Refrig., **24**(2), pp. 124–136.
[13] Douss, N., and Meunier, F., 1989, "Experimental Study of Cascading Adsorption Cycles," Chem. Eng. Sci., **44**(2), pp. 225–235.
[14] Misra, R. D., Sahoo, P. K., and Gupta, A., 2005, "Thermoeconomic Optimization of a LiBr/H2O Absorption Chiller Using Structural Method," ASME J. Energy Resour. Technol., **127**(2), pp. 119–124.
[15] Misra, R. D., Sahoo, P. K., and Gupta, A., 2006, "Thermoeconomic Evaluation and Optimization of an Aqua-Ammonia Vapour-Absorption Refrigeration System," Int. J. Refrig., **29**(1), pp. 47–59.
[16] Kizilkan, Ö., Şencan, A., and Kalogirou, S. A., 2007, "Thermoeconomic Optimization of a LiBr Absorption Refrigeration System," Chem. Eng. Process. Process Intensif., **46**(12), pp. 1376–1384.
[17] Kubota, M., Ueda, T., Fujisawa, R., Kobayashi, J., Watanabe, F., Kobayashi, N., and Hasatani, M., 2008, "Cooling Output Performance of a Prototype Adsorption Heat Pump With Fin-Type Silica Gel Tube Module," Appl. Therm. Eng., **28**(2–3), pp. 87–93.
[18] Jiangzhou, S., Wang, R. Z., Lu, Y. Z., Xu, Y. X., and Wu, J. Y., 2005, "Experimental Study on Locomotive Driver Cabin Adsorption Air Conditioning Prototype Machine," Energy Convers. Manage., **46**(9–10), pp. 1655–1665.
[19] Chua, H. T., Ng, K. C., Wang, W., Yap, C., and Wang, X. L., 2004, "Transient Modeling of a Two-Bed Silica Gel-Water Adsorption Chiller," Int. J. Heat Mass Transfer, **47**(4), pp. 659–669.
[20] Zhang, L. Z., 2000, "Design and Testing of an Automobile Waste Heat Adsorption Cooling System," Appl. Therm. Eng., **20**(1), pp. 103–114.
[21] Wang, R. Z., 2008, "Efficient Adsorption Refrigerators Integrated With Heat Pipes," Appl. Therm. Eng., **28**(4), pp. 317–326.
[22] Alahmer, A., Wang, X., Al-Rbaihat, R., Amanul Alam, K. C., and Saha, B. B., 2016, "Performance Evaluation of a Solar Adsorption Chiller Under Different Climatic Conditions," Appl. Energy, **175**, pp. 293–304.
[23] Chorowski, M., and Pyrka, P., 2015, "Modelling and Experimental Investigation of an Adsorption Chiller Using Low-Temperature Heat From Cogeneration," Energy, **92**, pp. 221–229.
[24] Huang, B. J., Chang, J. M., Petrenko, V. A., and Zhuk, K. B., 1998, "A Solar Ejector Cooling System Using Refrigerant R141b," Sol. Energy, **64**(4–6), pp. 223–226.
[25] Ma, X., Zhang, W., Omer, S. A., and Riffat, S. B., 2010, "Experimental Investigation of a Novel Steam Ejector Refrigerator Suitable for Solar Energy Applications," Appl. Therm. Eng., **30**(11–12), pp. 1320–1325.
[26] Murthy, S. S., Balasubramanian, R., and Murthy, M. V. K., 1991, "Experiments on Vapour Jet Refrigeration System Suitable for Solar Energy Applications," Renewable Energy, **1**(5–6), pp. 757–768.
[27] Dai, Y., Wang, J., and Gao, L., 2009, "Exergy Analysis, Parametric Analysis and Optimization for a Novel Combined Power and Ejector Refrigeration Cycle," Appl. Therm. Eng, **29**(10), pp. 1983–1990.
[28] Alexis, G. K., 2005, "Exergy Analysis of Ejector-Refrigeration Cycle Using Water as Working Fluid," Int. J. Energy Res, **29**(2), pp. 95–105.
[29] Xia, J., Wang, J., Lou, J., Zhao, P., and Dai, Y., 2016, "Thermo-Economic Analysis and Optimization of a Combined Cooling and Power (CCP) System for Engine Waste Heat Recovery," Energy Convers. Manage., **128**, pp. 303–316.
[30] Garousi Farshi, L., Mahmoudi, S. M. S., and Rosen, M. A., 2013, "Exergoeconomic Comparison of Double Effect and Combined Ejector-Double Effect Absorption Refrigeration Systems," Appl. Energy, **103**, pp. 700–711.
[31] Wang, H., Peterson, R., Harada, K., Miller, E., Ingram-Goble, R., Fisher, L., Yih, J., and Ward, C., 2011, "Performance of a Combined Organic Rankine Cycle and Vapor Compression Cycle for Heat Activated Cooling," Energy, **36**(1), pp. 447–458.
[32] Vélez, F., Segovia, J. J., Martín, M. C., Antolín, G., Chejne, F., and Quijano, A., 2012, "A Technical, Economical and Market Review of Organic Rankine Cycles for the Conversion of Low-Grade Heat for Power Generation," Renewable Sustainable Energy Rev, **16**(6), pp. 4175–4189.
[33] Yue, C., You, F., and Huang, Y., 2016, "Thermal and Economic Analysis of an Energy System of an ORC Coupled With Vehicle Air Conditioning," Int. J. Refrig., **64**, pp. 152–167.
[34] Gibson, S. C., Young, D., and Bandhauer, T. M., 2017, "Technoeconomic Optimization of Turbo-Compression Cooling Systems," International Mechanical Engineering Congress and Exposition, Tampa Bay, FL, pp. 1–17.
[35] Bandhauer, T. M., and Garland, S. D., 2016, "Dry Air Turbo-Compression Cooling," ASME Paper No. POWER2016-59152.
[36] Klein, S., and Alvarado, F., 2002, "Engineering Equation Solver," F-Chart Software, Box, Madison, WI.
[37] Nichols, K. E., *How to Select Turbomachinery for Your Application*, Barber-Nichols, Arvada, CO.
[38] Garland, S. D., Bandhauer, T. M., and Noall, J., 2017, "Performance Model of a Waste Heat Driven Turbo-Compression Chiller," Second Thermal and Fluids Engineering Conference, Las Vegas, NV, Paper No. TFEC-IWHT2017-18302.
[39] Kaelin, J., 2015, "Plate and Frame Heat Exchangers Explained," Thermaxx Jackets, West Haven, CT, accessed Dec. 1, 2017, https://www.thermaxxjackets.com/plate-and-frame-heat-exchangers-explained/
[40] Instrumentation and Process Control, 2011, "Advantages and Disadvantages of Plate Heat Exchangers," accessed Dec 1, 2017, http://instrumentations.blogspot.com/2011/04/advantages-and-disadvantages-of-plate.html
[41] Bergman, T. L., Lavine, A. S., Incropera, F. P., and Dewitt, D. P., 2011, *Fundamentals of Heat and Mass Transfer*, Wiley, Danvers, MA.
[42] Sinnott, R. K., 2005, *Chemical Engineering Design*, Butterworth-Heinemann, Oxford, UK, pp. 756–764.
[43] Kuo, W. S., Lie, Y. M., Hsieh, Y. Y., and Lin, T. F., 2005, "Condensation Heat Transfer and Pressure Drop of Refrigerant R-410A Flow in a Vertical Plate Heat Exchanger," Int. J. Heat Mass Transfer, **48**(25–26), pp. 5205–5220.
[44] Hsieh, Y. Y., and Lin, T. F., 2002, "Saturated Flow Boiling Heat Transfer and Pressure Drop of Refrigerant R-410A in a Vertical Plate Heat Exchanger," Int. J. Heat Mass Transfer, **45**(5), pp. 1033–1044.
[45] Thonon, B., Vidil, R., and Marvillet, C., 1995, "Recent Research and Developments in Plate Heat Exchangers," J. Enhanced Heat Transfer, **2**(1–2), pp. 149–155.
[46] Wanniarachchi, A. S., Ratman, U., Tilton, B. E., and Dutta-Roy, K., 1995, "Approximate Correlations for Chevron-Type Plate Heat Exchangers," 30th National Heat Transfer Conference, Portland, OR, Aug. 6–8, pp. 145–151.
[47] Rosenblad, G., and Kullendorff, A., 1975, "Estimating Heat Transfer Rates From Mass Transfer Studies on Plate Heat Exchanger Surfaces," Wärme Stoffübertragung, **8**(3), pp. 187–191.
[48] Heavner, H., Kumar, L., and Wanniarachchi, A. S., 1993, "Performance of an Industrial Plate Heat Exchanger: Effect of Chevron Angle," AIChE Symposium Series Heat Transfer, Atlanta, Georgia, Aug., pp. 262–267.
[49] Khan, T. S., Khan, M. S., Chyu, M.-C., and Ayub, Z. H., 2010, "Experimental Investigation of Single Phase Convective Heat Transfer Coefficient in a Corrugated Plate Heat Exchanger for Multiple Plate Configurations," Appl. Therm. Eng., **30**(8–9), pp. 1058–1065.
[50] Rajasekaran, S., and Raj, W. C., "Comparative Study of Nusselt Number for a Single Phase Fluid Flow Using Plate Heat Exchanger," Therm. Sci., **20**(Suppl. 4), pp. 929–935.
[51] Engineering ToolBox, 2004, "Minor Loss Coefficients in Pipe and Tube Components," accessed Dec. 1, 2017, http://www.engineeringtoolbox.com/minor-loss-coefficients-pipes-d_626.html
[52] Perry, R. H., 1997, *Chemical Engineers' Handbook*, McGraw-Hill, New York.
[53] Brown, T., 2007, *Engineering Economics and Economic Design for Process Engineers*, CRC Press, Boca Raton, FL.

[54] Vatavuk, W. M., 2002, "Updating the CE Plant Cost Index," Chem. Eng.-Eng. Pract., (epub).
[55] Garland, S. D., Bandhauer, T. M., Grauberger, A., Simon, J., Young, D., Fuller, R., Noall, J., Shull, J., Sami, R. V., Reinke, M. J., and Larry, W., 2018, "Experimental Investigation of a Waste Heat Driven Turbo-Compression Chiller," Third Thermal and Fluids Engineering Conference, Fort Lauderdale, FL, pp. 7–10.
[56] Couper, J., Penney, R., Fair, J., and Walas, S., 1990, *Chemical Process Equipment*, Butterworth-Heinemann, Newton, MA.
[57] Carrier, 2018, "Water-Cooled Chillers," United Technologies Corporation, Farmington, CT, accessed Dec. 1, 2017, https://www.carrier.com/commercial/en/us/products/chillers-components/water-cooled-chillers/
[58] Carrier, 2018, "Air-Cooled Chillers," United Technologies Corporation, Farmington, CT, accessed Dec. 1, 2017, https://www.carrier.com/commercial/en/us/products/chillers-components/air-cooled-chillers/
[59] Airedale, 2018, "Air Condition Chillers," Airedale Air Conditioning, Leeds, UK, accessed Dec. 1, 2017, http://airedale.com/web/Products/Chillers.htm
[60] Achaichia, N., 2011, "Working Fluid Developments for HT Heat Pumps and ORC Systems," Renewable Energy, Heating and Cooling Applications, Edinburgh, Scotland, Jan. 21, pp. 1–9.
[61] Bu, X. B., Li, H. S., and Wang, L. B., 2013, "Performance Analysis and Working Fluids Selection of Solar Powered Organic Rankine-Vapor Compression Ice Maker," Sol. Energy, **95**, pp. 271–278.
[62] Kim, K. H., and Perez-Blanco, H., 2015, "Performance Analysis of a Combined Organic Rankine Cycle and Vapor Compression Cycle for Power and Refrigeration Cogeneration," Appl. Therm. Eng, **91**, pp. 964–974.
[63] Li, H., Bu, X., Wang, L., Long, Z., and Lian, Y., 2013, "Hydrocarbon Working Fluids for a Rankine Cycle Powered Vapor Compression Refrigeration System Using Low-Grade Thermal Energy," Energy Build., **65**, pp. 167–172.